Optimal Perturbation Tolerance in VSC-Connected Hybrid Networks Using an Expert System on Chip

Brook W. Abegaz, *Member, IEEE*, and Satish M. Mahajan, *Senior Member, IEEE*

***Abstract*—A major challenge in the stable operation of hybrid power networks is that such systems operate under the influence of perturbations from source fluctuations and from dynamic storage operations. In the current practice, hybrid power networks are operated and controlled by higher-level supervisory control systems using approaches such as the droop control logic that may not make use of the accurate network models, full-state measurements, and learning mechanisms to deal with the convoluted perturbations on voltage source converters (VSCs). These perturbations could result from natural variations, parameter uncertainties, grid faults, variable loadings, controller settings, and other exogenous disturbances. So far, these perturbations have been considered as lumped terms that do not represent the correlation of perturbations across the network components. In this paper, an integrated, on-chip expert system (EXPSOC) is proposed to compute the correlation between power variables in separate modules, to perform state estimation of power and voltage variables and to improve the tolerance of perturbations in the hybrid networks. Results show the optimality of the approach in controlling dynamic power perturbations and in keeping the stability of the voltage, frequency, and power variables at the level of grid-connected VSCs.**

***Index Terms*—Converters, estimation, expert systems, observers, perturbation methods, stability.**

NOMENCLATURE

A. Perturbation Analysis on Source Converters

$u,\ x,\ y$	Input vector $u \in \mathbb{R}$, State vector $x \in \mathbb{R}$, and output vector $y \in \mathbb{R}$.
$f(x),\ g(x),\ h(x)$	Vector fields.
$V_a,\ V_b,\ V_c$	Three-phase, grid-side converter voltages.
$V_{de},\ V_{qe}$	d-axis and q-axis components of $V_a,\ V_b$, and V_c.
$i_a,\ i_b,\ i_c$	Three-phase grid currents.
i_d, i_q	d-axis and q-axis components of $i_a,\ i_b$, and i_c.
$V'_a,\ V'_b,\ V'_c$	Three-phase grid voltages.
$V'_{de},\ V'_{qe}$	d- and q-axis components of V'_a, V'_b, and V'_c
$w,\ C$	Angular speed of three-phase grid voltages and dc-link capacitance.
$R,\ L$	Equivalent resistance and inductance between the grid-side VSC and the grid transformer.
$V_{\text{dc}},\ i_{\text{dc}}$	Voltage and current of the dc-link capacitor.
$i_{\text{dc1}}, i_{\text{dc2}}$	Source-side and grid-side dc-link current.

B. Perturbation Analysis on Storage Converters

P_{VSC}	Power at the converter terminals.
$v_{\text{dclink}}, i_{\text{dc}}$	Dc-link voltage and the current to/from the dc–dc converter.
$v_{\text{dclink}-\text{ref}}$	Reference dc-link voltage.
v_d, i_d	Direct component of the voltage and current to/from the VSC.
v_q, i_q	Quadrature component of the voltage and current to/from the VSC.
m, ϕ	Modulation index, angle of Park's transformation.
d_1, d_2	Switching starting and ending intervals.
T_s	Operational period of the dc-dc converter.
$S_1,\ S_2$	MOSFET switches.
$C_1,\ C_2$	Input capacitance, dc-link capacitance.
L_4	Inductance between the storage unit and the connected VSC.
R_{load}	Equivalent resistance of the VSC and the grid.
$i_L,\ I_{\text{peak}}$	Inductor current and peak current.
$V_{\text{ESS}},\ R_{\text{ESS}}$	Voltage and internal resistance of storage units.
$x,\ \frac{dx}{dt}, \Delta x$	Error and differential error amounts.
Δi_L	Inductor current differential perturbation.
$\Delta v_{\text{in}}, \Delta v_{\text{dclink}}$	Input and dc-link voltage differential perturbation.

Manuscript received March 7, 2017; revised June 19, 2017; accepted July 18, 2017. Date of publication August 4, 2017; date of current version February 22, 2018. Recommended for publication by Associate Editor L. Peng. *(Corresponding author: Brook W. Abegaz.)*

B. W. Abegaz is with the Department of Engineering Science, Loyola University Chicago, Chicago, IL 60660 USA (e-mail: b.w.abegaz@ieee.org).

S. M. Mahajan is with the Department of Electrical and Computer Engineering and the Center for Energy Systems Research, Tennessee Technological University, Cookeville, TN 38505 USA (e-mail: smahajan@tntech.edu).

Color versions of one or more of the figures in this paper are available online at http://ieeexplore.ieee.org.

Digital Object Identifier 10.1109/TPEL.2017.2736002

See http://www.ieee.org/publications_standards/publications/rights/index.html for more information.

C. Differential and Algebraic Relations

$L_f h(x)$	Differentiation of h(x) with respect to f(x).
$B(x)$	Nominal control gain.
$y_i^{(n)}$, $\mathrm{y}_i^{\mathrm{est}}$, $\mathrm{y}_i^{\mathrm{init}}$, $\mathrm{y}_i^{\mathrm{meas}}$	nth derivative of output i and the estimated, initial and measured output values.
v_i	New inputs of the linearized system i.
α_{ij}, m_c, r	Power flow assortativity, power modularity, and number of lines with power flow L.
str_i	Strength of power flow on branch i.
$\frac{dV_{\mathrm{ref},i}}{dt}$	Reference voltage perturbations.
P_i, $F_{i,j}$	Power capacity and flow amount between terminals i and j.
k_{ij}, e_{ij}	Controller gains and related errors.
s, L	Modular group index and level of power flow.
$P_i P_i/2L$	Power flow between terminals i and j.
ψ_i, ψ_i^{est}	Perturbation of subnetwork i and its estimate.
$B_{\mathrm{i}}(x)$, $C_{\mathrm{i}}(x)$, $B(0)$, $C(0)$	Nominal control gain and perturbation propagation matrices and their initial values.

I. Introduction

The highly stochastic nature of voltage and power perturbations from hybrid sources and the dynamism of storage operations affect the stable and efficient operations of hybrid power networks. The perturbation problem is exacerbated by the presence of numerous operational entities, which have highly complex and real-time communication requirements. If a hybrid power network is subjected to imbalances, fluctuations, or external disturbances, the consequences could be rather severe, which include malfunctioning nodes [5], broken links [6], and even cascaded failures [7], [8]. Singular perturbations occurring in power systems have been widely addressed in the literature [1]–[6]. However, convoluted perturbations from multivariable, hybrid sources have not been fully addressed since such analysis may involve large system complexity and require highly dynamic computations. Unmatched convoluted perturbations are problematic in power networks that are largely composed of continually dynamic sources, which often are long distances apart to manage their stochasticity on an individual basis. The adverse effects of such perturbations could go from node imbalances to cascaded node and link failures. These severe results imply that there is a need for an active management mechanism using intelligent control methods as highlighted in [7] for power networks operating under nonlinear variabilities from multiple sources. Thus, for hybrid networks to be utilized in a dependable manner, their system characteristics need to be analyzed at the network interface level, and ways to improve stability need to be computed in near real-time domains.

The stability of power networks consisting of significant storage units has been investigated extensively in recent literature [8]–[11]. Nevertheless, hybrid power networks consisting of dc–dc and dc–ac converter connected storage systems that are exposed to multiple perturbations have not yet been investigated targeting improved perturbation tolerance. Such an analysis could be very useful in systems where the dynamic operation of grid-connected storage units such as plug-in electric vehicles could potentially introduce multiple perturbations that could go unresolved and may negatively affect the stability of the entire power network. In storage systems interfaced with a voltage source converter (VSC), perturbations related to the internal resistance, capacitance, and voltage of a storage system could affect the overall system stability. Whenever there are variations in the state of charge, depth of discharge (DoD), or usage frequencies of storage units, convoluted effects of the small multiple perturbations could have larger effects on stability. For instance, the equivalent series resistance of a storage unit could increase up to 130% when the storage unit is discharged at various DoD values or due to variations in ambient temperature [12]. Furthermore, although it is generally expected that storage systems could experience a lower degradation rate if they are subject only to fewer discharge cycle variations or perturbations, the amount of storage capacity degradation due to the exposure to a series of perturbations has not fully been addressed in the literature and has been left for future work in [12]. Literature in this research area has mainly focused on the study of systems consisting of a few operational converters [13], [14]. Various converter and inverter control strategies including the droop control logic method and signal injection method have been proposed in [15]–[17]. In some of these studies, the converters were modeled as ideal voltage sources without considering perturbations from dissipative impedances. Thus, the voltage and power dynamics that could represent perturbations at the converter terminals were not fully considered. In some other studies, stability analysis was performed offline without an integrated scheme that could provide prompt and logical responses to perturbations within small transition and propagation times.

Recent studies in this area have started using the artificial intelligence based approaches for power system operational analysis. These include analyzing the nontechnical losses in power systems [1], the active power curtailment, and overvoltage prevention in low-voltage feeders [2], and the robust control of distributed generation systems under voltage sags [3]. While most of these studies are based on learning and estimation based operations, they do not fully address the tolerance of power perturbations during disturbances and uncertainties. Moreover, the optimal perturbation tolerance approach for power networks is yet to be identified on the basis of comparative performance and reliability metrics. Such an approach could solve power perturbations at the points of common coupling or at the levels of the VSCs in the power network.

A knowledge-based expert system is a computational machine that emulates decision making in large-scale, complex

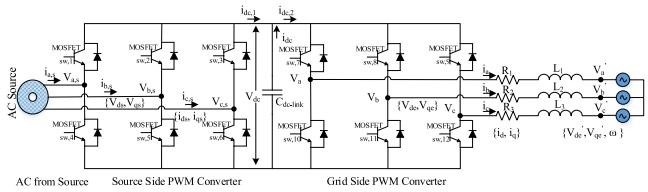

Fig. 1. VSC interconnection of an ac-source and the grid.

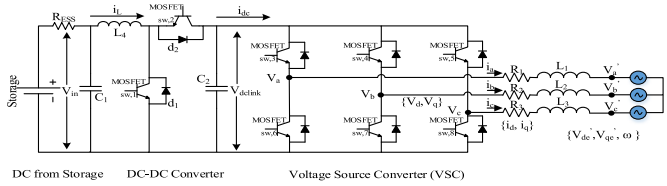

Fig. 2. VSC interconnection of a dc–dc converter based storage system and the power grid.

processes by observing the continuous changes in operational variables, building a set of conditions and developing well-defined tasks [18]. Challenges in hybrid networks related to multiple voltage, frequency, and real and reactive power perturbations could be resolved if optimal planning and control mechanisms are performed by using an integrated expert system. This paper presents such an integrated expert system approach. The proposed expert system provides real-time learning based solutions by using new spatiotemporal variables, which could be used to select the state of modulation of a group of power converters for optimal perturbation resistance in the power electronic network. Furthermore, the expert system compares and implements various algorithms to identify an optimal nonlinear control action within operating margins for perturbation tolerance in the network. This kind of expert system based perturbation resistance, resilience, and tolerance improvement of a VSC-connected hybrid power network has not yet been presented in the literature. Moreover, the extension of the proposed strategy to emerging hybrid network technologies is an anticipated advantage of the proposed integrated expert system approach.

II. Problem Formulation

Stability problems in power networks are related to the dynamic perturbations during the operations of sources, loads, and storage units. These perturbations could arise from natural variations, parameter uncertainties, grid faults, variable loadings, controller settings, and other exogenous disturbances, which have so far been considered to result in lumped perturbation terms that do not represent the correlation of perturbations across the network components. In hybrid networks, the normal operations of dc–dc, dc—ac, and ac–ac VSCs connected to sources, loads, and storage units are affected by the dynamic voltage, frequency, and power perturbations.

A. Perturbations on Source Connected VSC

A VSC connected ac-power source is shown in Fig. 1 [4]. The state model of the grid-side VSC and the dc-link capacitor is given in (1)–(7) [19], where the state vector $x \in \mathbb{R}$, the input vector $u \in \mathbb{R}$, the output vector $y \in \mathbb{R}$, and the vector fields $f(x)$, $g(x)$, and $h(x)$ are expressed in the relations. The three-phase grid side converter voltages V_a, V_b, and V_c have a d-axis component V_{de} and a q-axis component V_{qe}. The three-phase grid currents i_a, i_b, and i_c have a d-axis component i_d and a q-axis component i_q. The three-phase grid voltages V'_a, V'_b, and V'_c have a d-axis component V'_{de} and a q-axis component V'_{qe}, and an angular speed w. The resistance and inductance between the grid-side VSC converter and the grid-side transformer are given as R and L. The dc-link capacitor C has voltage and current values given as V_{dc} and i_{dc}. The source side dc-link current is given as i_{dc1} and the grid side dc-link current is given as i_{dc2}

$$\dot{x} = f(x) + g_1(x)\,u_1 + g_2(x)\,u_2 \tag{1}$$

$$x = \begin{bmatrix} i_d & i_q & V_{\text{dc}} \end{bmatrix}^T \tag{2}$$

$$f(x) = \begin{bmatrix} \frac{1}{L}V'_{de} - \frac{R}{L}i_d + w i_q \\ \frac{1}{L}V'_{qe} - \frac{R}{L}i_q - w i_d \\ \frac{3V'_{de}i_d}{2CV_{\text{dc}}} - \frac{i_{\text{dc2}}}{C} \end{bmatrix} \tag{3}$$

$$g_1(x) = \begin{bmatrix} -\frac{1}{L} & 0 & 0 \end{bmatrix}^T \tag{4}$$

$$g_2(x) = \begin{bmatrix} 0 & -\frac{1}{L} & 0 \end{bmatrix}^T \tag{5}$$

$$u = \begin{bmatrix} u_1 & u_2 \end{bmatrix}^T = \begin{bmatrix} V_{de} & V_{qe} \end{bmatrix}^T \tag{6}$$

$$y = \begin{bmatrix} y_1 & y_2 \end{bmatrix}^T = \begin{bmatrix} h_1(x) & h_2(x) \end{bmatrix}^T = \begin{bmatrix} i_q & V_{\text{dc}} \end{bmatrix}^T. \tag{7}$$

Source disturbances are represented by changes in the source side dc-link current i_{dc1} that could be caused due to the variable active power generated from the ac-source due to the variability of the connected sources. In addition, disturbances from load imbalances and grid faults could cause the dc-link voltage V_{dc} and the grid-side currents i_d and i_q to vary beyond safe limits.

B. Perturbations on Storage Connected VSC

Electronic interfaces for storage systems mainly consist of dc–dc converters and dc–ac VSCs that change the output voltage level or convert the dc-voltage to an ac-voltage. A three-phase VSC has been studied in the literature, where a generic model was developed as given in Fig. 2 [20]. The VSC transfers real power to or from the grid depending on the charging or discharging state of the storage system. The state of the storage unit determines if the phase angle of the converter leads or lags the phase angle of the connected grid. The amount of power P_{VSC} that flows in or out of the VSC is calculated from the dc-link voltage V_{dclink} and the dc current i_{dc} to or from the dc–dc converter as given in (8).

The fundamental frequency of the output voltage of the VSC is related to the dc-link voltage and the modulation index m of the VSC. The dc-link current is related to the direct i_d and quadrature i_q components of the output current of the VSC as

given in (9), and the amount of power transferred between the converter terminals and the grid is computed as given in (10)

$$P_{\text{VSC}} = V_{\text{dclink}} i_{\text{dc}} \tag{8}$$

$$i_{\text{dc}} = \frac{3}{4} m(\cos(\phi) i_q + \sin(\phi) i_d) \tag{9}$$

$$P_{\text{VSC}} = \frac{3}{2} \left(i_d V_d + i_q V_q \right). \tag{10}$$

Perturbations of the ac-side direct i_d and quadrature current i_q components affect the dc-side current and need to be balanced by changing the duty cycle of the dc–dc converter. On the other hand, high-frequency switching could result in voltage and current fluctuations and poses an instability problem. The state-space equations for the switching of the dc–dc converter relate the switching intervals d_1 and d_2 (11), the peak current I_{peak} in the operational period of the dc–dc converter T_s (12), (13), the inductor current i_L (14), (15), the equivalent resistance R_{load} of the VSC and the grid circuit it is connected to, the dc-link voltage V_{dclink} (16), the input voltage V_{in} (17), and their differential error (18) [11], [21]

$$\begin{bmatrix} \dfrac{di_L}{dt} \\ \dfrac{dV_{\text{dclink}}}{dt} \end{bmatrix} = \begin{bmatrix} 0 & -\dfrac{d_2}{L_4} \\ \dfrac{d_2}{C_2} & -\dfrac{1}{R_{\text{load}} C_2} \end{bmatrix} \begin{bmatrix} i_L \\ V_{\text{dclink}} \end{bmatrix} + \begin{bmatrix} \dfrac{d_1 + d_2}{L_4} \\ 0 \end{bmatrix} V_{\text{in}} \tag{11}$$

$$i_L = \frac{I_{\text{peak}}}{2} (d_1 + d_2) \tag{12}$$

$$I_{\text{peak}} = \frac{V_{\text{in}}}{L_4} d_1 T_s \tag{13}$$

$$d_2 = \frac{2 L_4 i_L}{d_1 T_s V_{\text{in}}} - d_1 \tag{14}$$

$$\frac{di_L}{dt} = \frac{2 L_4}{d_1 T_s} \left(\frac{V_{\text{dclink}}}{V_{\text{in}}} - 1 \right) - \frac{d_1 V_{\text{dclink}}}{L_4} \tag{15}$$

$$\frac{dV_{\text{dclink}}}{dt} = \frac{i_L}{C_2} - \frac{d_1^2 T_s V_{\text{in}}}{2 L_4 C_2} - \frac{V_{\text{dclink}}}{R_{\text{load}} C_2} \tag{16}$$

$$\frac{dV_{\text{in}}}{dt} = \frac{V_{\text{ESS}} - V_{\text{in}}}{R_{\text{ESS}} C_1} - \frac{i_L}{C_1} \tag{17}$$

$$\frac{dx}{dt} = V_{\text{dclink-ref}} - V_{\text{dclink}}. \tag{18}$$

Equation (11) could be written in a state-space model of the dc-link capacitor and the grid-side VSC as given in (19) and (20), where $u \in \mathbb{R}$ is the input vector in (21), $x \in \mathbb{R}$ is the state vector in (22), $y \in \mathbb{R}$ is the output vector in (20), $f(x)$, $g(x)$, and $h(x)$ are vector fields in (23)–(25)

$$\dot{x} = f(x) + g_1(x) u_1 + g_2(x) u_2 \tag{19}$$

$$y = h(x) = [V_{\text{dclink}}] \tag{20}$$

$$u = [V_{\text{in}}] \tag{21}$$

$$x = \begin{bmatrix} i_L & V_{\text{dclink}} \end{bmatrix}^T \tag{22}$$

$$f(x) = \begin{bmatrix} -\dfrac{d_2 V_{\text{dclink}}}{L_4} \\ \dfrac{d_2 i_L}{C_2 (d_1 + d_2)} - \dfrac{V_{\text{dclink}}}{R_{\text{load}} C_2} \end{bmatrix} \tag{23}$$

$$g_1(x) = \begin{bmatrix} \dfrac{(d_1 + d_2)}{L_4} & 0 \end{bmatrix}^T \tag{24}$$

$$g_2(x) = \begin{bmatrix} 0 & 0 \end{bmatrix}^T. \tag{25}$$

III. Linearization and Perturbation Estimation

The nonlinearity of the VSC systems described in the problem formulation in (1)–(7) and (19)–(25) could be linearized to estimate the interactions during perturbations. For a nonlinear, multiple-input, multiple-output (MIMO) system described using a control input vector $u \in \mathbb{R}$, an output vector $y \in \mathbb{R}$, a state vector $x \in \mathbb{R}$, and vector fields $f(x)$, $g(x)$, and $h(x)$, the output y could be differentiated until the input appears in order to linearize the system as given in (26)–(30) [22]. If the differentiation is performed n times using the Lie derivative approach [23], the input output relation could be described and the system i could be controlled as a linear system with new inputs of the system v_i and a nominal gain $B(x)$ as given in (31) and (32)

$$\frac{dy}{dt} = \dot{y} = \dot{h}(x) . \dot{x} = \frac{dh(x)}{dt} . f(x) + \frac{dh(x)}{dt} . g(x) u \tag{26}$$

$$L_f h(x) = \frac{dh(x)}{dt} . f(x) ; L_g h(x) = \frac{dh(x)}{dt} . g(x) \tag{27}$$

$$\dot{y} = L_f h(x) + L_g h(x) u \tag{28}$$

$$y_i^{(n)} = L_f^n h_i + \sum_{j=1}^{m} L_{g_j} L_f^{n-1} h_i u_j \tag{29}$$

$$\begin{bmatrix} y_1^{(n)} \\ \vdots \\ y_m^{(n)} \end{bmatrix} = \begin{bmatrix} L_f^n h_1 \\ \vdots \\ L_f^n h_m \end{bmatrix} + B(x)^* \begin{bmatrix} u_1 \\ \vdots \\ u_m \end{bmatrix} \tag{30}$$

$$B(x) = \begin{bmatrix} L_{g_1} L_f^{n-1} h_1 & \dots & L_{g_m} L_f^{n-1} h_1 \\ \vdots & \vdots & \vdots \\ L_{g_1} L_f^{n-1} h_m & \dots & L_{g_m} L_f^{n-1} h_m \end{bmatrix} \tag{31}$$

$$y_i^{(n)} = v_i. \tag{32}$$

A. Linearization on Source Connected VSC

For a MIMO source connected VSC system given in (1)–(7), the input output and feedback linearization could be performed by differentiating the output until the input appears; therefore, the nth derivative of the output could be computed as given in (26)–(30) to yield the following:

$$L_f^{(1)} h_1 = \frac{1}{L} V_{qe} - \frac{R}{L} i_q - w i_d \tag{33}$$

$$L_f^{(2)} h_1 = \left(\frac{3 V_{de} i_d}{2 C V_{\text{dc}}} - \frac{i_{\text{dc2}}}{C} \right)' = \frac{3 V_{de} \left(\frac{1}{L} V_{de} - \frac{R}{L} i_d + w i_q \right)}{2 C V_{\text{dc}}} - \frac{3 V_{de} i_d}{2 C V_{\text{dc}}^2} \left(\frac{3 V_{de} i_d}{2 C V_{\text{dc}}} - \frac{i_{\text{dc2}}}{C} \right) - \frac{(i_{\text{dc2}})'}{C} \tag{34}$$

$$B(x) = \begin{bmatrix} 0 & \left(\frac{R}{L} - w \right) / L \\ 3 V_{de} / 2 C L V_{\text{dc}} & 0 \end{bmatrix}. \tag{35}$$

The source connected VSC system could be linearized as given in (36)–(42) using new inputs of the system v_1 and v_2

$$\begin{pmatrix} u_1 \\ u_2 \end{pmatrix} = B(x)^{-1} \begin{pmatrix} -L_f^{(1)} h_1 + v_1 \\ -L_f^{(2)} h_1 + v_2 \end{pmatrix} \tag{36}$$

$$\dot{y}_1 = \left(\frac{1}{L} V_{qe} - \frac{R}{L} i_q - w i_d \right) + \left(\left(\tfrac{R}{L} - w \right) \Big/ L \right) u_1 \tag{37}$$

$$\ddot{y}_2 = \left(\frac{3V_{de} \left(\frac{1}{L} V_{de} - \frac{R}{L} i_d + w i_q \right)}{2CV_{\text{dc}}} - \frac{3V_{de} i_d}{2CV_{\text{dc}}^2} \left(\frac{3V_{de} i_d}{2CV_{\text{dc}}} - \frac{i_{\text{dc2}}}{C} \right) - \frac{(i_{\text{dc2}})'}{C} \right) + \left(3V_{de} / 2CLV_{\text{dc}} \right) u_2 \tag{38}$$

$$v_1 = \dot{y}_{1r} + k_{11} e_1 \tag{39}$$

$$v_2 = \ddot{y}_{2r} + k_{21} \dot{e}_2 + k_{22} e_2 \tag{40}$$

$$v_1 = \left(\frac{1}{L} V_{qe} - \frac{R}{L} i_q - w i_d \right) + \left(\left(\tfrac{R}{L} - w \right) \Big/ L \right) u_1 + k_{11} e_1 \tag{41}$$

$$v_2 = \left(\frac{3V_{de} \left(\frac{1}{L} V_{de} - \frac{R}{L} i_d + w i_q \right)}{2CV_{\text{dc}}} - \frac{3V_{de} i_d}{2CV_{\text{dc}}^2} \left(\frac{3V_{de} i_d}{2CV_{\text{dc}}} - \frac{i_{\text{dc2}}}{C} \right) - \frac{(i_{\text{dc2}})'}{C} \right) + \left(3V_{de} / 2CLV_{\text{dc}} \right) u_2 + k_{21} \dot{e}_2 + k_{22} e_2. \tag{42}$$

B. Linearization on Storage Connected VSC

For a MIMO storage connected VSC system given in (19)–(25), the input output and feedback linearization could be performed by differentiating the output until the input appears, therefore, the nth derivative of the output could be written given as

$$\begin{aligned} L_g L_f^{n-1} h_1 &= \nabla \left(L_f^{n-1} h_1 \right) . g = \frac{\partial}{\partial x} \left(L_f^{n-1} h_1 \right) . g_1 (x) \\ &= \frac{\partial}{\partial i_L} \left(L_f^{n-1} h_1 \right) . g_1 (x) + \frac{\partial}{\partial V_{\text{dclink}}} \left(L_f^{n-1} h_1 \right) . g_1 (x) . \end{aligned} \tag{43}$$

To calculate the control gain matrix $B(x)$ given in the form of (31) for the storage connected VSC system, (44) to (48) are used

$$\begin{aligned} L_f h = h.f = \frac{\partial h}{\partial x} . f &= \frac{dV_{\text{dclink}}}{di_L} \begin{bmatrix} 0 & -\frac{d_2 V_{\text{dclink}}}{L_4} \\ \frac{d_2 i_L}{C_2 (d_1 + d_2)} & -\frac{V_{\text{dclink}}}{R_{\text{load}} C_2} \end{bmatrix} \\ &+ \frac{dV_{\text{dclink}}}{dV_{\text{dclink}}} \begin{bmatrix} 0 & -\frac{d_2 V_{\text{dclink}}}{L_4} \\ \frac{d_2 i_L}{C_2 (d_1 + d_2)} & -\frac{V_{\text{dclink}}}{R_{\text{load}} C_2} \end{bmatrix} \\ &= \begin{bmatrix} 0 & -\frac{d_2 V_{\text{dclink}}}{L_4} \\ \frac{d_2 i_L}{C_2 (d_1 + d_2)} & -\frac{V_{\text{dclink}}}{R_{\text{load}} C_2} \end{bmatrix} \end{aligned} \tag{44}$$

$$L_{g_1} L_f^0 h = L_{g_1} h = \frac{\partial h}{\partial x} . g_1 = \frac{(d_1 + d_2)}{L_4} \tag{45}$$

$$L_{g_2} L_f^0 h = 0 \tag{46}$$

$$\begin{aligned} L_{g_1} L_f^1 h = \frac{d}{dx} \left[\frac{\partial h}{\partial x} f \right] . g_1 &= \frac{d}{dx} \left[\frac{\partial V_{\text{dclink}}}{\partial i_L} f + \frac{\partial V_{\text{dclink}}}{\partial V_{\text{dclink}}} f \right] . g_1 \\ = \frac{d}{dx} \begin{bmatrix} 0 & -\frac{d_2}{L_4} V_{\text{dclink}} \\ \frac{d_2 i_L}{C_2 (d_1 + d_2)} & -\frac{V_{\text{dclink}}}{R_{\text{load}} C_2} \end{bmatrix} . g_1 &= \begin{bmatrix} 0 & 0 \\ \frac{d_2}{C_2 (d_1 + d_2)} & 0 \end{bmatrix} . g_1 \\ + \begin{bmatrix} 0 & -\frac{d_2}{L_4} \\ 0 & -\frac{1}{R_{\text{load}} C_2} \end{bmatrix} . g_1 &= \begin{bmatrix} 0 & -\frac{d_2}{L_4} \\ \frac{d_2}{C_2 (d_1 + d_2)} & -\frac{1}{R_{\text{load}} C_2} \end{bmatrix} \\ \cdot \begin{bmatrix} \frac{(d_1 + d_2)}{L_4} & 0 \end{bmatrix}^T &= \frac{d_2}{C_2 L_4} \end{aligned} \tag{47}$$

$$B(x) = \begin{bmatrix} (d_1 + d_2) / L_4 \\ d_2 / C_2 L_4 \end{bmatrix} . \tag{48}$$

The derivatives of the output are then calculated as given in (49)–(52), whereas the inputs of the linearized storage connected VSC system are calculated as given in (53) and (54).

$$F_1 (x) = -\frac{d_2 V_{\text{dclink}}}{L_4} \tag{49}$$

$$F_2 (x) = \frac{d_2}{C_2 (d_1 + d_2)} - \frac{1}{R_{\text{load}} C_2} \tag{50}$$

$$\dot{y}_1 = -\frac{d_2 V_{\text{dclink}}}{L_4} + \left(\frac{(d_1 + d_2)}{L_4} \right) u_1 \tag{51}$$

$$\ddot{y}_2 = \frac{d_2}{C_2 (d_1 + d_2)} - \frac{1}{R_{\text{load}} C_2} + \left(\frac{d_2}{C_2 L_4} \right) u_2 \tag{52}$$

$$v_1 = \left(-\frac{d_2 V_{\text{dclink}}}{L_4} + \left(\frac{(d_1 + d_2)}{L_4} \right) u_1 \right) + k_{11} e_1 \tag{53}$$

$$v_2 = \left(\frac{d_2}{C_2 (d_1 + d_2)} - \frac{1}{R_{\text{load}} C_2} + \left(\frac{d_2}{C_2 L_4} \right) u_2 \right) + k_{21} \dot{e}_2 + k_{22} e_2. \tag{54}$$

C. Perturbation Observer

For a perturbation vector ψ and nominal control gain $B(0)$, the source and storage connected VSC system equations could be related to the amount of perturbation. The perturbation observer modeled in this paper is as given in (55). This observer is unique in that it calculated the propagated amounts of perturbation $C(x)$ from the power network variables into the estimated perturbation at the converter terminals as given in (55). The system equations could be written using the computed perturbation term as given in (56)

$$\begin{bmatrix} \psi_1 (x) \\ \psi_2 (x) \end{bmatrix} = \begin{bmatrix} L_f^n h_1 \\ L_f^n h_2 \end{bmatrix} + \begin{bmatrix} B_1 (x) - B_1 (0) \\ B_2 (x) - B_2 (0) \end{bmatrix} \begin{bmatrix} u_1 \\ u_2 \end{bmatrix} + \begin{bmatrix} C_1 (x) - C_1 (0) \\ C_2 (x) - C_2 (0) \end{bmatrix} \tag{55}$$

$$\begin{bmatrix} y_1^n \\ \vdots \\ y_m^n \end{bmatrix} = \begin{bmatrix} \psi_1 \\ \vdots \\ \psi_m \end{bmatrix} + [B(0)] * \begin{bmatrix} u_1 \\ \vdots \\ u_m \end{bmatrix} + [C(0)] . \tag{56}$$

The perturbation observer performs a new technique, where new network analysis based perturbation computation is performed for converters in power modules. The new estimates of the subsystem variables $\mathrm{y}_i^{\mathrm{est}}$ and their derivatives are computed in (57)–(59) using the power assortativity and power modularity variables in (60) and (61). The power flow assortativity coefficient is a correlation coefficient between the weighted flows of all branches between nodes. A positive power flow assortativity coefficient indicates that nodes are connected to other nodes with similar power flow characteristics. This relation is used to determine the propagation of perturbations across the hybrid network, where the correlation of power flow profiles could indicate the strength of connection between nodes. The power flow assortativity α_{ik} of converter terminals i and k is calculated as given in (60) from the sum of power flow strengths of lines between i and k as compared to the total r lines in the power network. The power modularity m_c of converters has been identified for connected regions (61), where L is the power capacity level in the network, F_{ij} is the branch power flow between terminals i and j, P_i is the power capacity of terminal i, $\frac{P_i P_j}{2L}$ is the expected power flow with in level L between terminals i and j, s is the grouping index of the module M_c, where $s_i = 1$ if the terminal i is a member of the power module M_c or $i \epsilon M_c$

$$\dot{\mathrm{y}}_{i1}^{\mathrm{est}} = \dot{\mathrm{y}}_{i2}^{\mathrm{est}} + \sum_{\forall k \in m_c} \alpha_{ik} * \left(y_{k1} - \mathrm{y}_{k1}^{\mathrm{est}}\right) \tag{57}$$

$$\dot{\mathrm{y}}_{\mathrm{in}}^{\mathrm{est}} = y_{i(n)} + \sum_{\forall k \in m_c} \alpha_{ik} * \left(y_{k1} - \mathrm{y}_{k1}^{\mathrm{est}}\right) + B_{ko} u + C_{ko} \tag{58}$$

$$\psi_i^{\mathrm{est}} = \dot{\mathrm{y}}_{i(n+1)}^{\mathrm{est}} = \sum_{\forall k \in m_c} \alpha_{ik} * \left(y_{ki} - \mathrm{y}_{ki}^{\mathrm{est}}\right) \tag{59}$$

$$\alpha_{ik} = \frac{\left(\frac{\sum (str_i * str_k)}{r} - \left(\frac{\sum \left(\frac{1}{2} * (str_i + str_k)\right)}{r}\right)^2\right)}{\left(\frac{\sum \left(\frac{1}{2} * (str_i + str_k)\right)}{r} - \left(\frac{\sum \left(\frac{1}{2} * (str_i + str_k)\right)}{r}\right)^2\right)} \tag{60}$$

$$m_c = \frac{1}{4L} \sum_{i=1}^{N} \sum_{j=1}^{N} (F_{ij} - \frac{P_i P_j}{2L}) s_i s_j. \tag{61}$$

IV. Perturbation Tolerance Using Expert System on Chip (EXPSOC)

A. Perturbation Tolerance Approaches

There are various approaches used in the literature for the tolerance of perturbations in the context of VSC-connected hybrid networks. These include feedback linearizing control (FLC), adaptive nonlinear controller (ANC), vector control and learning-based approaches including artificial neural network based control (ANN), and fuzzy logic based approaches. FLC has been used to generate a complex nonlinear control law using a full system model, a full-state feedback of all the measured variables. ANC has been used to reduce the controller complexity without requiring a detailed system model nor a full-state feedback. Learning-based approaches, such as a fuzzy logic based, ANN-based, or optimization-based approaches could be used to take decisions based on measurements. However, the decision levels may not be updated in the real time, which could create inaccuracies in real-time operations. In addition, the power relations of the network components may not be efficiently represented while observing or estimating perturbations and efficient remedies may not be taken.

An expert system could form a knowledge-base for a detailed and accurate system model of the hybrid network and could compute a full-state feedback of all the necessary variables. It has advantages over the other competing approaches in that it could build its knowledge base on both the changes on the converter voltage and power variables and on the correlation of power network variables. The EXPSOC approach provides a larger database to store such information and could create a more realistic identification of perturbation cause-and-effect relations to take optimal and real-time control decisions and actions.

B. Nonlinear Perturbation Tolerance

Using the proposed expert system, nonlinear perturbations could be tolerated by using a control input vector u that is computed from the output feedback vector v, the computed perturbation vector ψ and the control gain matrix in (35) and (48) as given in (62). The nonlinear perturbation tolerance for source and storage connected VSC systems is performed by using new control input vectors that are calculated from output feedbacks of the perturbation observer

$$\begin{aligned} u &= B_0^{-1} \left\{ \begin{bmatrix} v_1 \\ \vdots \\ v_m \end{bmatrix} - \begin{bmatrix} \psi_1^{\mathrm{est}} \\ \vdots \\ \psi_m^{\mathrm{est}} \end{bmatrix} \right\} \\ &= B_0^{-1} \left\{ \begin{bmatrix} v_1 \\ \vdots \\ v_m \end{bmatrix} - \begin{bmatrix} \sum\limits_{\forall k \in m_c} \alpha_{1k} * \left(y_{k1} - \mathrm{y}_{k1}^{\mathrm{est}}\right) \\ \vdots \\ \sum\limits_{\forall k \in m_c} \alpha_{mk} * \left(y_{km} - \mathrm{y}_{km}^{\mathrm{est}}\right) \end{bmatrix} \right\}. \end{aligned} \tag{62}$$

C. Perturbation Tolerance on Source VSC

For the system given in (1)–(7), the derivatives of the output and the outputs of the linearized system are calculated in (36)–(42). Substituting in the final control law yields the control input vectors as follows:

$$\begin{aligned} u_1 = \frac{2 V_{\mathrm{dc}} C_0 L_0}{3 V_{de}} \Big(&- \psi_2^{\mathrm{est}} + k_{22} \left(V_{\mathrm{dc}r} - V_{\mathrm{dc}}\right) \\ &+ k_{21} \left(\dot{V}_{\mathrm{dc}r} - y_{22}^{\mathrm{est}}\right) + \ddot{V}_{\mathrm{dc}r} \Big) \end{aligned} \tag{63}$$

$$u_2 = - L_0 \left(-\psi_1^{\mathrm{est}} + k_{11} \left(i_{qr} - i_q\right) + \ddot{i}_{qr}\right). \tag{64}$$

D. Perturbation Tolerance on Storage VSC

For the system given in (19)–(25), the derivatives of the output and the outputs of the linearized system are calculated in (49)–(54). Substituting in the final control law yields the control

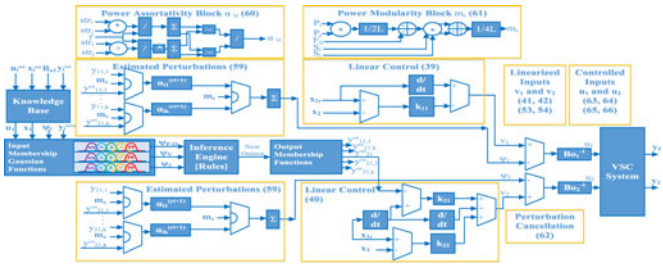

Fig. 3. Block diagram of the EXPSOC.

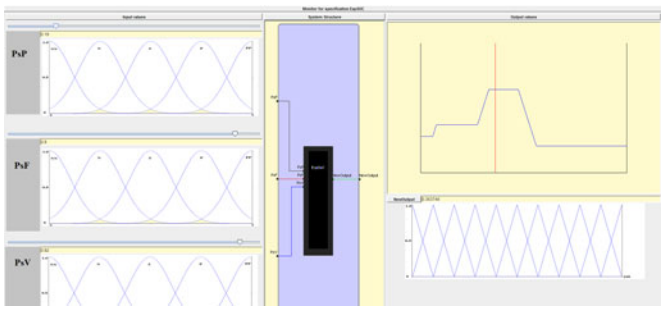

Fig. 4. Implementation of input power, voltage, and angle perturbations and output Gaussian membership functions

input vectors as follows:

$$u_1 = \frac{L_4}{(d_1+d_2)}\left(\psi_1^{\text{est}} + \left(\left(\frac{(d_1+d_2)}{L_4}\right)v_1 - \frac{d_2 V_{\text{dclink}}^{\text{est}}}{L_4}\right) + k_{11}e_1\right) \tag{65}$$

$$u_2 = \frac{C_2 L_4}{d_2}\left(\psi_2^{\text{est}} + \left(\frac{d_2}{C_2\,(d_1+d_2)} - \frac{1}{R_{\text{load}}C_2} + \left(\frac{d_2}{C_2 L_4}\right)v_2\right) + k_{21}\dot{e}_2 + k_{22}e_2\right) \tag{66}$$

E. Proposed Expert System on Chip

A functional block diagram of the design of the proposed EXPSOC is shown in Fig. 3 consisting of three main components: a knowledge-base (memory), an inference engine (processor), and a control unit. EXPSOC has sets of input and output Gaussian membership functions, rules of inference, and a look-up table used to classify convoluted perturbations, as shown in Figs. 4–6. It implements variable membership functions, rules and associations using reconfigurable blocks on chip so that estimates of perturbations are adjusted in real time. In addition, EXPSOC consists of a power assortativity and a power modularity computational blocks, which are used to compute the network power flow relations and the propagation of perturbations. The processor relates the nonlinear inputs with the power variables to compute the inputs of the linearized system v_{i} that cancel the estimated perturbations ψ_i^{est}.

Three new algorithms have been implemented on EXPSOC, namely an estimation-based (EXPSOC-EST), fitness-based (EXPSOC-FIT), and interlacing-based (EXPSOC-INT) perturbation tolerance, and an optimal implementation of the three algorithms, labeled (EXPSOC-OPT). The estimation-based algorithm was based on perturbation estimation based on the previous time-step inputs, outputs, and system variables. The fitness-based algorithm was based on estimation based on the average perturbation on inputs and system variables. The interlacing-based approach implemented perturbation estimation based on differential changes of perturbation based on the last two outputs of the implementation. The optimal algorithm (EXPSOC-OPT) could select and implement the algorithm that has been implemented on the EXPSOC that resulted in the higher perturbation tolerance at every time step of implementation.

Rule			Premise		Conclusion
0	1.0	if	(PsP == NN & PsF == NN & PsV == NN)	->	NewOutput = hundredth
1	1.0	if	(PsP == NN & PsF == NN & PsV == N)	->	NewOutput = hundredth
2	1.0	if	(PsP == NN & PsF == NN & PsV == Z)	->	NewOutput = hundredth
3	1.0	if	(PsP == NN & PsF == NN & PsV == P)	->	NewOutput = hundredth
4	1.0	if	(PsP == NN & PsF == NN & PsV == PP)	->	NewOutput = hundredth
5	1.0	if	(PsP == NN & PsF == N & PsV == NN)	->	NewOutput = ninetieth
6	1.0	if	(PsP == NN & PsF == N & PsV == N)	->	NewOutput = eightieth
7	1.0	if	(PsP == NN & PsF == N & PsV == Z)	->	NewOutput = eightieth
8	1.0	if	(PsP == NN & PsF == N & PsV == P)	->	NewOutput = eightieth
9	1.0	if	(PsP == NN & PsF == N & PsV == PP)	->	NewOutput = ninetieth
10	1.0	if	(PsP == NN & PsF == Z & PsV == NN)	->	NewOutput = ninetieth
11	1.0	if	(PsP == NN & PsF == Z & PsV == N)	->	NewOutput = eightieth
12	1.0	if	(PsP == NN & PsF == Z & PsV == Z)	->	NewOutput = eightieth
13	1.0	if	(PsP == NN & PsF == Z & PsV == P)	->	NewOutput = eightieth
14	1.0	if	(PsP == NN & PsF == Z & PsV == PP)	->	NewOutput = ninetieth
15	1.0	if	(PsP == NN & PsF == P & PsV == NN)	->	NewOutput = ninetieth
16	1.0	if	(PsP == NN & PsF == P & PsV == N)	->	NewOutput = eightieth
17	1.0	if	(PsP == NN & PsF == P & PsV == Z)	->	NewOutput = eightieth
18	1.0	if	(PsP == NN & PsF == P & PsV == P)	->	NewOutput = eightieth
19	1.0	if	(PsP == NN & PsF == P & PsV == PP)	->	NewOutput = ninetieth
20	1.0	if	(PsP == NN & PsF == PP & PsV == NN)	->	NewOutput = hundredth
21	1.0	if	(PsP == NN & PsF == PP & PsV == N)	->	NewOutput = hundredth
22	1.0	if	(PsP == NN & PsF == PP & PsV == Z)	->	NewOutput = hundredth
23	1.0	if	(PsP == NN & PsF == PP & PsV == P)	->	NewOutput = hundredth
24	1.0	if	(PsP == NN & PsF == PP & PsV == PP)	->	NewOutput = hundredth
25	1.0	if	(PsP == N & PsF == NN & PsV == NN)	->	NewOutput = seventieth
26	1.0	if	(PsP == N & PsF == NN & PsV == N)	->	NewOutput = seventieth
27	1.0	if	(PsP == N & PsF == NN & PsV == Z)	->	NewOutput = seventieth
28	1.0	if	(PsP == N & PsF == NN & PsV == P)	->	NewOutput = seventieth
29	1.0	if	(PsP == N & PsF == NN & PsV == PP)	->	NewOutput = seventieth
30	1.0	if	(PsP == N & PsF == N & PsV == NN)	->	NewOutput = sixtieth

Fig. 5. EXPSOC rules of inference implementation.

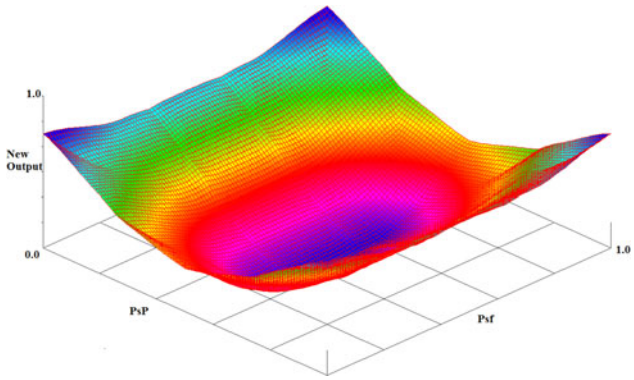

Fig. 6. Surface plot of the control function for increasing power and frequency perturbations.

V. Experimental Setup

A diagram of the experimental setup of the EXPSOC with a power grid-connected, VSC-interfaced sources, storage units, and loads in hybrid power networks is shown in Fig. 7. The power flow variables of voltage, angle, real, and reactive power are gathered by EXPSOC from both terminals of the VSC. The processor of the EXPSOC computes estimates of perturbations based on the spatiotemporal variability of the voltage, angle, and power variables from the computed power flows as compared to the values that have been stored in the database. The control

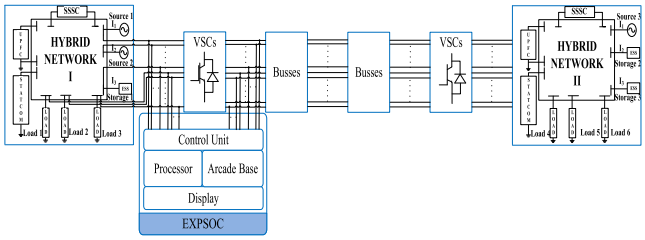

Fig. 7. Diagram depicting the experimental setup using the integrated expert system-on-chip (EXPSOC).

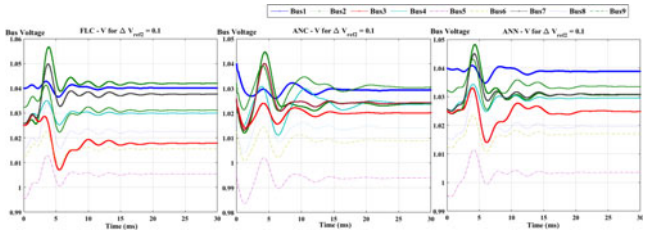

Fig. 8. Stability of bus voltages after convoluted perturbations in approaches using (a) FLC, (b) ANC, (c) ANN.

unit sets the VSC variables according to the optimal perturbation tolerance decision.

On the experiments, a test system consisting of three generating sources and nine busses having 100-MVA base and 60-Hz frequency has been used. The generator, exciter, and governor parametric values have been set according to a practical power grid network based on data obtained from the Western System Coordinating Council (WSCC), which has been used in the literature [24]. For the sources, three 1-MW wind power generators have been interfaced as shown in Fig. 1 using a VSC having a d-axis component of three-phase grid-side converter voltages $V_{de}\ (0) =\ 690$ V, a d-axis and a q-axis components of three-phase grid currents $i_d\ (0) = -966.18$ A, and $i_q\ (0) = 0$ A, a dc-link capacitor C voltage $V_{\rm dc}\ (0) = 1050$ V, and a grid side dc-link current $i_{\rm dc2} = -1000$ A. For verification, these values were set to be the same as those that have been used in [4]. For the storage units, the inductor current $i_L = 188.5$ A, the average dc-link voltage $V_{\rm dclink} = 600$ V, the input voltage $V_{\rm in} = 132$ V, the voltage and the resistance of the storage unit $V_{\rm ESS} = 255$ V and $R_{\rm ESS} = 0.49\ \Omega$ were used. For verification purposes, these values were set to be the same as the ones used for experimentation in [11]. The system shown in Fig. 2 had parameters of $L_4 = 368\ \mu$H, $f_s = 2$ kHz, $R_{\rm load} = 14.4\ \Omega$, $V_{\rm dclink} = 600$ V, $P_{\rm max} = 25$ kW, and $C_{1,2} = 20$ mF.

VI. Results and Discussion

The proposed EXPSOC was implemented for the voltage and power stability of a nine-bus power network with three sources and three storage units. The results were compared with competing approaches from the literature. A comparison of the stability of bus voltages after 10% of reference voltage perturbations is shown in Fig. 8, where control approaches namely FLC, ANC, ANN are compared with the EXPSOC that implemented three new algorithms on the expert system on chip.

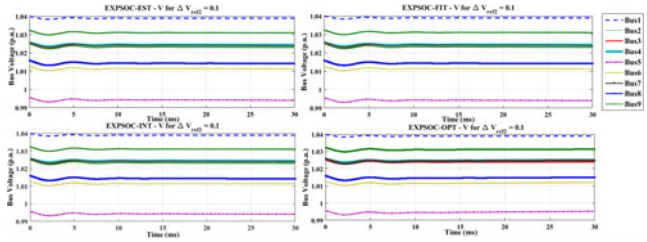

Fig. 9. Stability of bus voltages using EXPSOC algorithms (a) Estimation, (b) Fitness, (c) Interlacing, and (d) Optimal.

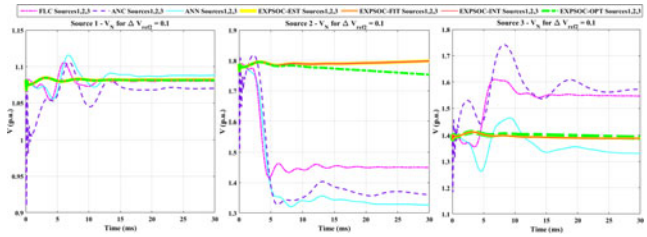

Fig. 10. Source 1, 2, 3 converter voltages in FLC, ANC, ANN, and EXPSOC algorithms (Estimation, Fitness, Interlacing, Optimal).

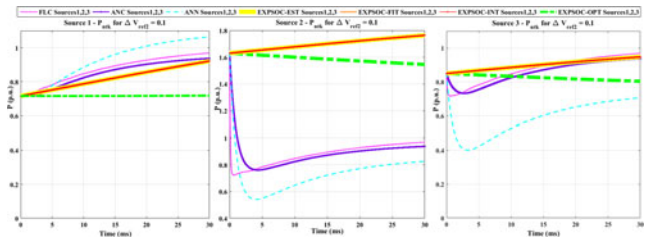

Fig. 11. Real power from sources 1, 2, 3 in FLC, ANC, ANN, and EXPSOC algorithms (Estimation, Fitness, Interlacing, and Optimal).

It was observed in Fig. 8 that a 4.4% per unit perturbation on the converter terminal voltage at 0.25 ms was cleared at 15 ms using the FLC approach, whereas similar bus voltage stability was observed at 25 ms for both the adaptive nonlinear controller and the ANN implementation. Using the EXPSOC with three different algorithms, the introduced 4.4% per unit VSC voltage perturbations were cleared before the 5th ms at the bus terminal voltages as shown in Fig. 9 (a)–(d), showing that the propagation time of convoluted perturbations could be decreased by at least 33.3% using the expert system. Moreover, it was observed that the clearance time of perturbations was synchronized across all busses using the integrated expert system approach as compared to the other competing approaches shown in Fig. 8. For the perturbations on the external power, VSC voltage perturbations showed similar exponential stability behavior as shown in Fig. 10 (a)–(c). It could be seen that only the expert system based approaches exhibited both the exponential and asymptotic stabilities on the power variables, whereas the other approaches of feedback linearizing control, adaptive linearizing control, and neural network approaches showed higher divergence during external power perturbations as observed in Figs. 10 and 11.

An experimental comparison of the seven approaches has been performed considering the bus voltages, angles and the machine voltages and currents as shown in Table I. The

TABLE I
COMPARISON OF THE APPROACHES

Method And Variable	FLC	ANC	ANN	EXPSOC-EST	EXPSOC-FIT	EXPSOC-INT	EXPSOC-OPTIMAL
Bus Voltage	0 to 1050 V in 100 s	0 to 1100 V in 100 s	0 to 800 V in 100 s	0 to 1100 V in 100 s	0 to 750 V in 100 s	0 to 1050 V in 100 s	0 to 750 V in 100 s
Machine Voltage	0 to 1050 V in 100 s	0 to 1100 V in 100 s	0 to 800 V in 100 s	0 to 1100 V in 100 s	0 to 750 V in 100 s	0 to 1050 V in 100 s	0 to 750V in 100 s
E_{dp}	-0.32 to -0.8 V in 10 s	-0.32 to -0.8 V in 10 s	-0.32 to -0.75 V in 10 s	-0.32 to -0.8 V in 10 s	-0.32 to -0.72 V in 10 s	-0.32 to -0.78 V in 10 s	-0.32 to -0.72 V in 10 s
E_{fd}	4 to 6.5 V and 1.8 V in 10 s	4 to 7 V and 2 V in 10	3 to 5 V and 1.5 V in 10 s	3 to 6.5 V and 1.8 V in 10 s	1.5 to 4.2 V and 1.5 V in 10 s	3 to 1V and 1.8 V in 10 s	1.5 to 4.2 and 1.5 V in 10 s
E_{qp}	1 to 2 V and 1.85 V in 10 s	1 to 2.1 V and 1.7 V in 10 s	1 to 1.75 V and 1.6 V in 10 s	1 to 2 V and 1.9 V in 10 s	1 to 1.65 V and 1.5 V in 10 s	1 to 2 V and 1.8 V in 10 s	1 to 1.65 V and 1.5 V in 10 s
I_d	0.7 to 0.2 A in 10 s	1 to -0.2 A in 10 s	1 to 0.2 A in 10 s	0.7 to 0.2 A in 10 s	0.7 to 1 A and -0.2 A in 10 s	0.6 to -0.3 A and 0.2 A in 10 s	1 to 0.25 A in 10 s
I_q	-1 to -0.4 A in 10 s	-1 to -0.4 A in 10 s	-1 to -0.25 A in 10 s	-1 to -0.4 A in 10 s	-1 to -0.3 A in 10 s	-1 to -0.4 A in 10 s	-1 to -0.25 A in 10 s
P_{sv}	0 to -0.6 W in 10 s	0 to -0.6 W in 10 s	0 to -0.4 W in 10 s	0 to -0.6 W in 10 s	0 to -0.4 W in 10 s	0 to -0.55 W in 10 s	0 to -0.4 W in 10 s
R_f	0.2 to 1.1 Ω and 0.3 Ω in 10 s	0.4 to 1.1 Ω and 0.3 Ω in 10 s	0.2 to 0.8 Ω and 0.3 Ω in 10 s	0.2 to 1.1 Ω and 0.3 Ω in 10 s	0.2 to 0.72 Ω and 0.3 Ω in 10 s	0.2 to 1.1 Ω and 0.3 Ω in 10 s	0.2 to 0.3 Ω and 0.3 Ω in 10 s
T_M	0/s to -0.6/s in 10 s	0/s to -0.6/s in 10 s	0/s to -0.4/s in 10 s	0/s to -0.6/s in 10 s	0/s to -0.4/s in 10 s	0/s to -0.55/s in 10 s	0/s to -0.4/s in 10 s
V	1.1 to 2.2 V and 2.0 V in 10 s	1.1 to 2.2 V and 2.0 V in 10 s	1.1 to 1.9 V and 1.7 V in 10 s	1.1 to 2.2 V and 2.0 V in 10 s	1.1 to 1.8 V and 1.6 V in 10 s	1.1 to 2.2 V and 1.8 V in 10 s	1.1 to 1.8 V and 1.6 V in 10 s
$V_R ss$	9 to 2 V in 10 s	9 to 2 V in 10 s	7 to 1.5 V in 10 s	9 to 2 V in 10 s	4 to 6 V and 1.5 V in 10 s	9 to 1 V in 1.8 s	4 to 6 V and 1.5 V in 10 s
ω	60 to 62 Hz in 10 s	60 to 62 Hz in 10 s	60 to 61.5 Hz in 10 s	60 to 61.8 Hz in 10 s	60 to 61 Hz in 10 s	60 to 62 Hz in 10 s	60 to 61 Hz in 10 s

experimental results are in agreement with the results obtained using simulation. In all of the experiments, the EXPSOC-optimal approach resulted in an optimal perturbation tolerance that resulted in smaller changes after the occurrence of a perturbation. The stability of the source machine variables was improved: the bus voltage stability was improved up to 23.81%, with similar effects on the generator machine voltages, the direct and quadrature machine voltages (E_{dp} and E_{qp}), the field voltage (E_{fd}), the direct and quadrature machine currents (I_d and I_q), the controller settings (P_{sv}, R_f), the reference voltage (V_R), and the machine frequency (ω) as shown in Table I.

Moreover, the advantages of using the integrated expert system were observed in localizing perturbations in voltage, angle, and real and reactive power amounts. This was achieved by weighting the variability of node profiles that are on the line of perturbation propagation. The profiles of directly connected nodes were correlated in an assortative order as computed by the expert system; therefore, bifurcation of regions that are stable, quasi-stable or marginally stable could be investigated. Transition and propagation times of fluctuations could be predicted and their amplitudes could be limited. As a result, the amount of storage that needed to be utilized to tolerate perturbations could be properly maintained.

VII. CONCLUSION

Perturbation tolerance of converter connected hybrid networks has been presented using a knowledge-based approach based on reference voltage, power, frequency, and angle relations of the VSC connected sources and storage units operating under convoluted perturbations. An integrated expert system has been used to select the optimal operating conditions that resulted in the desired perturbation tolerance characteristics in VSC connected hybrid networks. The knowledge-based estimation approach could be essential when the mathematical model of the control process is not available, or when the computation of exact perturbations is computationally too expensive. The direct impact of the expert system on chip approach is resolving the influence of perturbations from source fluctuations and from dynamic storage operations in hybrid power networks, and increasing the efficiency of converter operations and the effective utilization of resources. The approach could also be a basis for real-time monitoring of multiple single-level and advanced multilevel voltage source converters in the future. In addition, the reconfigurability of the expert system by updating its inference with new rules and membership functions is an advantage over competing approaches, and makes the system to be implementable on a single chip.

REFERENCES

[1] I. Dobson and E. Barocio, "Perturbations of weakly resonant power system electromechanical modes," *IEEE Trans. Power Syst.*, vol. 20, no. 1, pp. 330–337, Feb. 2005.
[2] P. Bhowmik, D. Rajan, S. Das, and A. Indira, "Power perturbation method for power flow analysis," *Int. J. Autom. Power Eng.*, vol. 1, pp. 1–5, 2012.
[3] J. Kimball and P. Krein, "Singular perturbation theory for DC–DC converters and application to PFC converters," *IEEE Trans. Power Electron.*, vol. 23, no. 6, pp. 2970–2981, Nov. 2008.

[4] J. Chen, L. Jiang, W. Yao, and Q. Wu, "Perturbation estimation based nonlinear adaptive control of a full-rated converter wind turbine for fault ride-through capability enhancement," *IEEE Trans. Power Syst.*, vol. 29, no. 6, pp. 2733–2743, Nov. 2014.
[5] J. Yang, B. Wu, S. Li, and X. Yu, "Design and qualitative robustness analysis of an DOBC approach for DC-DC buck converters with unmatched circuit parameter perturbations," *IEEE Trans. Circuits Syst. I, Reg. Papers*, vol. 63, no. 4, pp. 551–560, Apr. 2016.
[6] Z. Jing, R. Wang, L. Chen, and J. Deng, "Attractive regions in power systems by singular perturbation analysis," in *Trends in Mathematics: Differential Equations With Symbolic Computation*, Basel, Switzerland: Birkhauser, 2006, pp. 121–142.
[7] J. A. P. Lopes, N. Hatziargyriou, J. Mutale, P. Djapic, and N. Jenkins, "Integrating distributed generation into electric power systems: A review of drivers, challenges and opportunities," *Electr. Power Syst. Res.*, vol. 77, pp. 1189–1203, 2007.
[8] K. Mehran, D. Giaouris, and B. Zahawi, "Stability analysis and control of nonlinear phenomena in boost converters using model-based takagi-sugeno fuzzy approach," *IEEE Trans. Circuits Syst. I: Reg. Papers*, vol. 57, no. 1, pp. 200–212, Jan. 2010.
[9] Y. Yao, F. Fassinou, and T. Hu, "Stability and robust regulation of battery-driven boost converter with simple feedback," *IEEE Trans. Power Electron.*, vol. 26, no. 9, pp. 2614–2626, Sep. 2011.
[10] J. Shiau and C. Ma, "Li-Ion battery charging with a buck-boost power converter for a solar powered battery management system," *Energies*, vol. 6, no. 3, pp. 1669–1699, 2013.
[11] D. Bazargan, S. Filizadeh, and A. Gole, "Stability analysis of converter-connected battery energy storage systems in the grid," *IEEE Trans. Sustain. Energy*, vol. 5, no. 4, pp. 1204–1212, Oct. 2014.
[12] J. Dogger, B. Roossien, and F. Nieuwenhout, "Characterization of Li-Ion batteries for intelligent management of distributed grid-connected storage," *IEEE Trans. Energy Convers.*, vol. 26, no. 1, pp. 256–263, Mar. 2011.
[13] S. Lee, G. Son, and J. Park, "Power management and control for grid-connected DGs with intentional islanding operation of inverter," *IEEE Trans. Power Syst.*, vol. 28, no. 2, pp. 1235–1244, May 2013.
[14] J. P. Lopes, C. L. Moreira, and A. G. Madureira, "Defining control strategies for micro-grid islanded operation," *IEEE Trans. Power Syst.*, vol. 21, no. 2, pp. 916–924, May 2006.
[15] J. Guerrero, L. d. Vicuña, J. Matas, M. Castilla, and J. Miret, "A wireless controller to enhance dynamic performance of parallel inverters in distributed generation systems," *IEEE Trans. Power Electron.*, vol. 19, no. 5, pp. 1205–1213, Sep. 2004.
[16] C. Sao and P. Lehn, "Autonomous load sharing of voltage source converters," *IEEE Trans. Power Deliv.*, vol. 20, no. 2, pp. 1009–1016, Apr. 2005.
[17] C. Chang, D. Gorinevsky, and S. Lall, "Dynamical and voltage profile stability of inverter-connected distributed power generation," *IEEE Trans. Smart Grid*, vol. 5, no. 4, pp. 2093–2105, Jul. 2014.
[18] C. T. Leondes, *Expert Systems: The Technology of Knowledge Management and Decision Making for the 21st Century*, vol. 6, San Diego, CA, USA: Academic, 2002, pp. 1–22.
[19] A. Mullane, G. Lightbody, and R. Yacamini, "Wind-turbine fault ride-though enhancement," *IEEE Trans. Power Syst.*, vol. 20, no. 4, pp. 1929–1937, Nov. 2005.
[20] P. Krause, O. Wasynczuk, and S. Sudhoff, *Analysis of Electric Machinery and Drive Systems*, Piscataway, NJ, USA: IEEE Press, 2002.
[21] J. Sun, D. Mitchell, M. Greuel, P. Krein, and R. Bass, "Averaged modeling of PWM converters operating in discontinuous conduction mode," *IEEE Trans. Power Electron.,* vol. 16, no. 4, pp. 482–492, Jul. 2001.
[22] L. Jiang, Q. Wu, and J. Y. Wen, "Decentralized nonlinear adaptive control for multimachine power systems via high-gain perturbation observer," *IEEE Trans. Circuits Syst. I, Reg. Papers*, vol. 51, no. 10, pp. 2052–2059, Oct. 2004.
[23] C. Li, X. Yu, T. Huang, G. Chen, and X. He, "A generalized hopfield network for nonsmooth constrained convex optimization: Lie derivative approach," *IEEE Trans. Neural Netw. Learn. Syst.*, vol. 27, no. 2, pp. 308–321, Feb. 2016.
[24] P. W. Sauer and M. A. Pai, *Power System Dynamics and Stability*, Upper Saddle River, NJ, USA: Prentice-Hall, 1998.

Brook W. Abegaz (S'12–M'16) received the Master of Science degree in computer engineering from Delft University of Technology (TU Delft), Netherlands in 2012, and the Ph.D. degree in electrical and computer engineering from Tennessee Technological University (TTU), USA in 2016.

He has worked as a research and development engineer at two research centers at TTU. In 2015, he has worked as a trainee memory design engineer on the development of a new type of non-volatile memory technology at Intel Corporation in California. Currently, he is an assistant professor at the Department of Engineering Science at Loyola University Chicago. His research interests include modern electronic systems, sensor technologies, smart power grids, and network based intelligent and expert systems.

Satish M. Mahajan (S'86–M'87–SM'09) received the B.E. degree in electrical engineering from the University of Poona, Pune, India, in 1978, the M.S. degree in electrical engineering from the State University of New York at Buffalo, Buffalo, NY, USA, in 1983, and the Ph.D. degree in electrical engineering from the University of South Carolina, Columbia, SC, USA, in 1987.

Since 1987, he has been the faculty of the Electrical and Computer Engineering Department, Tennessee Technological University (TTU), Cookeville, TN, USA. Currently he is the Director of the Center for Energy Systems Research (CESR) at the TTU. His research interests include the physical phenomena of optoelectronic and HV devices, and modeling of conventional and renewable power systems.